Received: 18 November 2019 | Revised: 8 January 2020 | Accepted: 14 January 2020

DOI: 10.1002/aic.16918

AIChE JOURNAL

EDITOR'S CHOICE: SEPARATIONS: MATERIALS, DEVICES AND PROCESSES

Amine-functionalized ordered mesoporous silicas as model materials for liquid phase acid capture

Peter J. Miller | Daniel F. Shantz

Department of Chemical and Biomolecular Engineering, Tulane University, New Orleans, Louisiana

Correspondence
Daniel F. Shantz, Department of Chemical and Biomolecular Engineering, Tulane University, 6823 St. Charles Avenue, New Orleans, LA 70118.
Email: dshantz@tulane.edu

Abstract

Uptake of dilute aqueous acetic acid was compared using primary, secondary, tertiary amines, and quaternary ammonium grafted ordered mesoporous silica. Primary amine and quaternary ammonium grafted samples showed the highest uptake, 0.21 mmol acetic acid/g SBA-15, with secondary and tertiary amines showing nominally lower, 0.18 mmol/g, at 0.5 mmol aminosilane loaded per gram SBA-15. Solution conditions during uptake were varied to conclude that only associated acetic acid could be bound and that the mechanism relied heavily on electrostatic interactions. The aminosilane packing density was found to be crucial to performance with variation depending on the ligand bulk as well as the silica support's pore size. Relevant solution conditions for cellulose depolymerization were also explored by comparing uptake of multiple organic acids and with dextrose added. Here, it was shown that the most hydrophobic organic acid was preferentially extracted, and the uptake was enhanced in the presence of dextrose.

KEYWORDS

acetic acid, amino silane chemistry, biomass, hybrid materials, MCM-41, SBA-15, solid–liquid extraction

1 | INTRODUCTION

Organic–inorganic hybrid materials are an intellectually interesting and technologically important class of matter. By combining the desirable properties of both hard and soft matter, it is possible to design materials with superior mechanical, thermal, optical, and chemical properties.[1-7] One subgroup of hybrid materials are amine-functionalized silicas.[1,8-11] This class of hybrids, where simple amine groups, often propylamine groups, are grafted to the silica surface have been explored for many applications. Carbon dioxide capture has received the most attention,[12,13] as the carbon dioxide uptake of these materials has been well studied under a variety of conditions and both the basic physical[12,14] and engineering properties[15,16] of these materials have been well determined. These studies are not limited to primary amines, with gas-phase CO_2 capture,[17-20] hazardous molecule capture,[21-23] and catalysis[24] compared with secondary and tertiary amines as well. Additionally, these materials have been used as liquid sorbents of hazardous metal ions,[25-27] dyes,[28] and other waste molecules[29-32] as well as of organic acids[33] and aromatic compounds[34] relevant to biomass production.

Converting cellulosic biomass (corn stover, switch grass, woodchips, and so on) into fuel for energy production or chemical upgrading is ideally a carbon neutral process.[35-40] However, it suffers from the high energy input needed for chemical separation and recovery. Cellulose depolymerization, which can be achieved by pyrolysis,[37,41-45] hydrolysis,[46] or gasification, is an inherently non-selective process.[47] In particular, hydrolysis produces dilute (defined here as 10 vol% or less) quantities of organic acids that are detrimental to subsequent processing steps. Organic acids removal often uses liquid aliphatic amine extractants and the mechanism of acid removal processes has been extensively studied by varying the pH,[48-51] concentration,[52,53] and temperature[54,55] on pure and mixed organic acid systems.[56-59] Extractions have been reported with primary,[50,51,55] tertiary,[48,50-55,57-61] and quaternary[48,59,61,62] aliphatic amine based extractants. The main factors governing the extraction process have been reported as extractant basicity,[49,60] acidity of organic acid,[51]

extractant polarity,[61] organic acid polarity,[30] diluent polarity,[34,49,57-59] and ability to anion exchange.[62] However, due to organic diluents required for the extractants to be soluble, the many component system is complicated to characterize and requires a potentially energy intensive separation. The use of solid sorbents could potentially eliminate this challenge. In addition, solid sorbents have been utilized in many separation processes[13] to reduce energy consumption by eliminating distillation or a solvent regeneration step. Liquid amines in particular also have the disadvantage of being caustic causing an increase in materials handling costs and decrease equipment longevity, which solid sorbents amine sorbents would improve.[63]

Here we study propylamine groups with varying degrees of methylation supported on ordered mesoporous silica (OMS) as a model system for understanding acetic acid capture using a solid sorbent. Acetic acid is a common component of processed biomass streams, and thus represents an interesting and technologically relevant target for removal from liquid streams. Depending on the initial biomass feed composition and the pretreatment method,[64,65] acetic acid concentration can vary, but is typically at or below 10 wt%. Accordingly, this work will focus on relatively dilute concentrations of acetic acid that would be applicable to other relevant biomass molecules or to more general dilute capture applications, such as water purification. How propylamine methylation, solution conditions, and the presence of competitor molecules affect the uptake of acetic acid is described.

2 | EXPERIMENTAL

2.1 | Materials

Tetraethoxysilane (TEOS, 99.9%) and (1-hexadecyl) trimethylammonium bromide (CTAB, 98%) were purchased from Alfa Aesar. 2 M hydrochloric acid (HCl), 0.5 M sulfuric acid (H_2SO_4), sodium hydroxide (NaOH), sodium acetate trihydrate (NaAc), sodium chloride (NaCl), and toluene were purchased from BDH (ACS reagent grade). Pluronic P123 ($EO_{20}PO_{70}EO_{20}$, MW = 5,800), (3-aminopropyl)trimethoxysilane (APTMS, 99%), (3-iodopropyl)trimethoxysilane (IPTMS, 97%), butyric acid (99%), hexanoic acid (99%), and dextrose were purchased from Sigma-Aldrich. *N*-methylaminopropyltrimethoxysilane (MAPTMS, 99%) and (*N*,*N*-dimethyl-3-amino)propyltrimethoxysilane (DMAPTMS,99%) were purchased from Gelest. ACS grade methanol was purchased from EMD Millipore. N® sodium silicate (28.7 wt% SiO_2, SiO_2/Na_2O = 3.22 [weight]) was provided by the PQ corporation. Trimethylamine (TMA, 4.2 M in ethanol) was provided by Acros Organics. ACS grade glacial acetic acid was purchased from AMRESCO. Toluene was purified using an MBRAUN MB-SPS solvent purification system. All other chemicals were used as received.

2.2 | OMS synthesis

The protocol reported by Zhao and coworkers[66] was used for SBA-15 synthesis. 13.18 g of Pluronic P123 were dissolved in 395 ml of 2 M HCl and 82 ml of deionized water by stirring for 5 hr at room temperature until the solution was clear without any solid surfactant visible. 28 g of TEOS were then added to that solution and stirred for 24 hr at 35°C in a water bath. The mixture was then placed into an oven at 80°C for 24 hr under static conditions. The mixture was then cooled, the solid products filtered, washed with deionized water, and dried at 80°C overnight. The solid products were then calcined to remove the Pluronic. The calcination procedure was as follows: the air-dried samples were heated from room temperature to 100°C at a rate of 1°C/min; held at 100°C for 2 hr; subsequently increased from 100 to 550°C at a rate of 1°C/min; and then held at 550°C for 8 hr.

MCM-41 was synthesized using the synthesis procedure of Edler and White.[67] As an example, 15.8 g of sodium silicate solution were added to a Teflon vessel, and mixed with 75.2 ml deionized water. Then, 0.54 g of solid NaOH were added to the solution followed by the addition of 14.58 g CTAB. The sample was stirred for 1 hr at room temperature. Subsequently, 31.2 ml of 0.5 M H_2SO_4 were added to this and stirred for 15 min at room temperature. The mixture was then placed in an oven at 100°C for 24 hr under static conditions. After 24 hr the sample was taken from the oven, cooled down to room temperature, and 1.0 N H_2SO_4 was added to the solution dropwise to adjust the pH to approximately 10. The sample was then put back in the oven at 100°C. The titration step was performed two additional times in regular 24-hr intervals. The total heating period was 96 hr. The mixture was then cooled, the solid products filtered, washed with deionized water, and dried at 80°C overnight. The solid products were then calcined to remove the organic molecule used in synthesis. The calcination procedure was as follows: the air-dried samples were heated from room temperature to 100°C at a rate of 1°C/min; held at 100°C for 2 hr; subsequently increased from 100 to 550°C at a rate of 1°C/min; and then held at 550°C for 8 hr.

2.3 | Synthesis of amine-functionalized OMS

Amine-functionalized SBA-15 and MCM-41 were prepared by post-synthetic grafting. An aliquot of APTMS, MAPTMS, or DMAPTMS (87, 99, and 109 μl for 0.5 mmol, respectively) was added to 1 g of calcined SBA-15 or MCM-41 in 100 ml of anhydrous toluene under argon. This mixture was stirred overnight in a closed container at room temperature. The product was collected by filtration, washed sequentially with toluene, methanol, deionized water, and then dried under vacuum for 24 hr.

For the quaternary ammonium grafted sample, an aliquot of IPTMS (99 μl for 0.5 mmol) was added to 1 g of calcined SBA-15 or MCM-41 in 100 ml of anhydrous toluene under argon. The flask was covered to prevent light exposure and stirred overnight. Then 5 ml of 4.2 M TMA in ethanol was added and stirred for 24 hr. The product was collected by filtration, washed sequentially with toluene, methanol, deionized water, and then dried under vacuum for 24 hr. The sample was then stirred in 100 ml of 100 mM NaCl for 2 hr then collected by filtration, washed sequentially with methanol, deionized water, and then dried under vacuum for 24 hr. Scheme 1 shows the silica surface of the four samples after amine grafting.

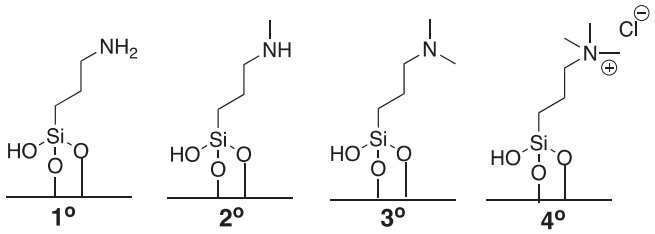

SCHEME 1 Cartoon depicting the various grafted silanes used in this work

2.4 | Acid uptake on grafted OMS

Grafted SBA-15 or MCM-41(0.1 g) was added to a 11 ml vial and mixed with 2 ml of aqueous acid solution. The slurry was mixed for 2 hr then centrifuged at 5,000 rpm for 10 minutes. The supernatant was then removed and filtered with a 0.45 μm cellulose acetate syringe filter. For the experiments performed where the pH was varied, 0.087 M sodium acetate (NaAc) was used to adjust the pH of a 0.087 M acetic acid solution to the desired value. For experiments that investigated the effect of dextrose and salt on acetic acid uptake the desired amount of dextrose or salt was added to a 0.087 M acetic acid solution.

Equilibrium concentrations were determined using high-performance liquid chromatography (HPLC) on an Agilent 1,260 Infinity fitted with a Hamilton PRP-1 Polymeric Reversed Phase Column. A mobile phase flow rate of 0.6 ml/min and the absorbance at 210 nm on a UV-vis detector was used for all measurements. The mobile phase varied based on experiments as follows, for solutions with only acetic acid, 5 mM H_2SO_4, for mixed acid solutions, a gradient of 5 mM H_2SO_4/acetonitrile (100/0–50/50 from 0 to 15 min then 50/50–100/0 from 15 to 17 min), and for pH adjusted samples, 50 mM H_2SO_4. The HPLC injections were done in triplicate for each experimental point. Uptake was calculated with Equation (1) where C_0 is initial concentration, C_{eq} is equilibrium concentration, m is mass of powder used, and V is volume of the solution.

Calculation of the equilibrium uptake as follows:

$$q_e = \frac{C_0 - C_{eq}}{\frac{m}{V}} \quad (1)$$

2.5 | Analytical methods

X-ray diffraction patterns were collected using a Rigaku MiniFlex 600 instrument. Thermogravimetric analysis (TGA) measurements were conducted on a TA Q500 instrument over a temperature range of 25–600°C and a ramp rate of 1°C/min. Nitrogen adsorption experiments were measured on a Micromeritics ASAP 2020 instrument using approximately 50 mg of sample. Prior to analysis the samples were degassed at 100°C for 24 hr. The mesopore volume and surface area was determined from the α_s-method. The mesopore size distributions were calculated from the desorption branch of the isotherms using the Barrett–Joyner–Halenda with a modified equation for statistical film thickness.

3 | RESULTS AND DISCUSSION

3.1 | OMS characterization

Figure 1 shows the powder X-ray diffraction (PXRD) patterns and the nitrogen adsorption isotherms of the parent SBA-15 and MCM-41. The patterns show the characteristic (100), (110), and (200) peaks of the hexagonally ordered pore structure of SBA-15[68] as well as the (100), (110), (200), and (220) of the MCM-41.[69] The decrease in the MCM-41 (100) reflection intensity for the amino-functionalized samples (Figures S1 and S2) is consistent with prior literature that shows upon incorporation of an organic layer one observes an attenuation of the reflections.[33,70] This signal attenuation is not due to any disruption of the ordering of the pores. Transmission electron microscopy (Figures S3–S5) is consistent with this conclusion. A list of the mesopore volumes for SBA-15 samples (Table S1) as well as pore distributions and nitrogen adsorption isotherms are shown in Figures S6–S9. A silane loading of 0.5 mmol/g loading was chosen to ensure uniform coverage of the various sizes and charges of the functional groups. Previous literature[71,72] states that 4 molecules/nm^2 for similar molecules to APTMS is the theoretical max loading for monolayer coverage, with 0.5 mmol/g being close to the max loading for the calculated surface area of SBA-15. However, it should be noted that practically much higher ligand loading has been obtained and that surface functionalization is likely not a monolayer due to heterogeneities on the silica surface.[73]

3.2 | Pure acetic acid uptake

Figure 2a shows the acetic acid uptake for a suite of aminosilicas (0.5 mmol/g) containing primary, secondary, tertiary amines and quaternary ammonium groups (denoted 1°, 2°, 3°, and 4°, respectively) using a 0.5 vol% (0.087 M) solution of acetic acid, which has an initial solution pH of 3.15. The primary and quaternary materials took up the most acetic acid, whereas the secondary and tertiary amines took up less acetic acid. The primary amine sample captured 0.21 mmol of acetic acid per gram of silica, corresponding to 0.42 mmol of acetic acid per mmol of amine group. This equated to 12% of the acetic acid removed from solution. The actual ligand loadings for the samples, calculated from TGA weight loss curves (Figure S10), were comparable to the theoretical loading (±5%) except for the quaternary sample which had a loading that was 70% of theoretical. Experiments performed with multiple samples made using the same protocols (Table S2) gave very similar results, indicating the results in Figure 2 were reproducible.

Figure 2b shows the uptake curves for the samples. Consistent with the results in Figure 2a, at low acetic acid concentrations there were differences between the various ligands. These differences

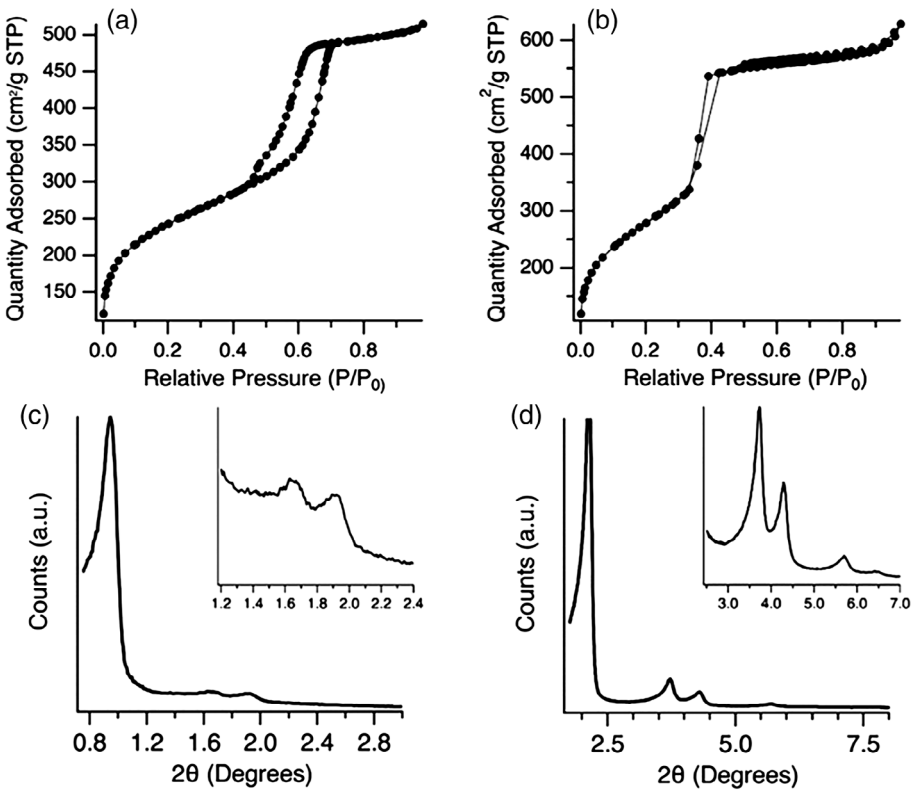

FIGURE 1 (a) Nitrogen adsorption isotherm of pristine SBA-15 (b) nitrogen adsorption isotherm of pristine MCM-41 (c) PXRD pattern of pristine SBA-15 with the inset showing magnification on the (110) and (200) reflections. (d) PXRD pattern of pristine MCM-41 with the inset showing magnification on the (110), (200), and (220) reflections

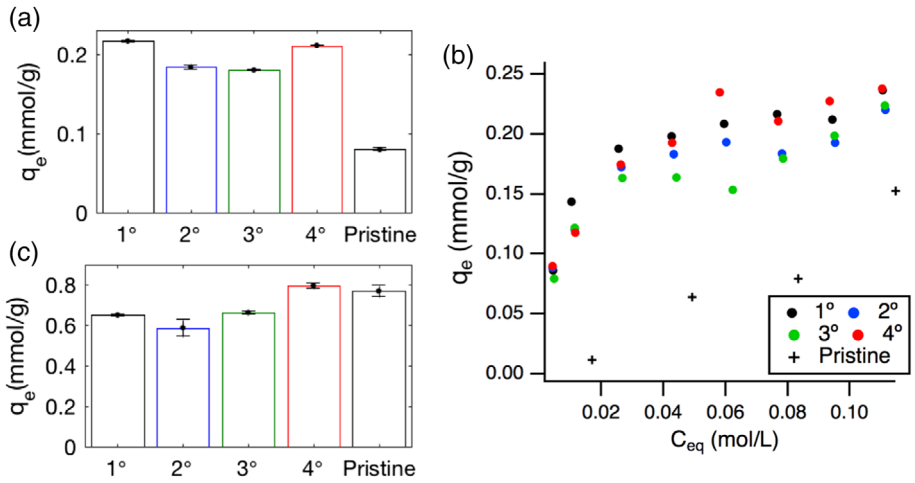

FIGURE 2 (a) Uptake of acetic acid from a 0.5 v% (0.087 M) solution on a series of aminosilicas with a nominal aminosilane loading of 0.5 mmol/g on SBA-15. (b) Uptake isotherm comparing the four amine functional groups loaded at 0.5 mmol/g on SBA-15. (c) Uptake of acetic acid from a 5 v% (0.87 M) solution on a series of aminosilicas with a nominal aminosilane loading of 0.5 mmol/g on SBA-15 [Color figure can be viewed at wileyonlinelibrary.com]

become less apparent at higher concentration. The bare, that is, non-functionalized SBA-15 is also shown in Figure 2 for comparison. At higher concentrations, uptake on bare SBA-15 converged to the grafted samples as seen in Figure 2c with an initial acetic acid concentration of 5 vol%. Bare SBA-15 uptake was likely due to hydrogen bonding of the surface silanol groups with the acetic acid —OH group. The increase in uptake as a function of concentration was due to clustering of acetic acid with an increase in concentration. This had been observed for other organic molecules with —OH groups.[74,75] Additionally, it should be noted that for all experiments only the bulk concentration of acid was monitored and it was assumed there was little volume change due to adsorption of the solute and solvent. As noted in recent literature,[76] these assumptions are important aspects of accurately quantifying batch adsorption experiments and since the concentrations in this work are dilute these assumptions likely hold. However, at higher concentrations a more rigorous approach to probe the adsorbed acid on the adsorbents surface would likely be required.

TABLE 1 Calculated fitting parameters for Langmuir and Freundlich fits of acetic acid uptake on amine-functionalized SBA-15 ($C_{eq} \leq 0.1$ M)

	Langmuir model			Freundlich model		
	K_L (L/Mol)	q_m (mmol/g)	χ^2	K_F	n	χ^2
1°	147.3 ± 6.7	0.234 ± 0.002	5.1×10^{-4}	0.398 ± 0.028	0.231 ± 0.022	5.6×10^{-3}
2°	152.2 ± 16.1	0.204 ± 0.004	2.0×10^{-3}	0.347 ± 0.023	0.227 ± 0.020	3.9×10^{-3}
3°	146.1 ± 19	0.193 ± 0.005	2.7×10^{-3}	0.336 ± 0.024	0.237 ± 0.023	3.7×10^{-3}
4°	90.4 ± 14.1	0.248 ± 0.009	5.9×10^{-3}	0.485 ± 0.035	0.301 ± 0.023	4.8×10^{-3}

$$\chi^2 = \sum_i \left(\frac{y - y_i}{\sigma_i} \right)^2$$

To further study the nature of the interaction, the adsorption isotherm data was fit using the Langmuir and Freundlich absorption models at low concentrations (<0.1 M) to minimize the effects of the nonselective uptake observed over bare SBA-15 at higher acetic acid concentrations. The Langmuir isotherm is given by the following equation[77]:

$$q_e = \frac{q_m K_L C_{eq}}{1 + K_L C_{eq}}$$

where q_m is maximum adsorption capacity (mmol/g) and K_L is the equilibrium adsorption constant related to the adsorption energy (L/mol). The Freundlich isotherm is represented by the following equation[78]:

$$q_e = K_F (C_{eq})^n$$

where K_F is a constant related to the adsorption capacity and n is a constant related to intensity. The results of the fits for the grafted aminosilane isotherms from Figure 2b are shown in Table 1. Neither model does an exceptional job fitting the data; however based purely on the χ^2 values the Langmuir model offers a slightly better fit. Given that the fits are comparable for both models in terms of the quality, one simple explanation for this is that at very low concentrations binding is primarily on amine groups, but because the amine grafting process leads to an uneven distribution (i.e., not monolayer) of surface tethered amine groups, the materials are heterogeneous which is likely the reason for the Langmuir model fit's shortcomings. This is further confounded by the well-known heterogeneity of the SBA-15 surface, for example, roughness, presence of microporosity in the walls, etc. The model fits on the experimental isotherm data can be seen in Figure S11.

For the amine-grafted samples the uptake mechanism was an acid–base interaction leading to near monolayer coverage at low concentrations. However, because there are still exposed surface silanol groups on the grafted samples, at acetic acid concentrations above 200 mM the primary extraction mechanism became similar to bare SBA-15. Finally, the kinetics of uptake were rapid in that the system equilibrates in less than 15 min for all cases based on transient uptake measurements (Figure 3).

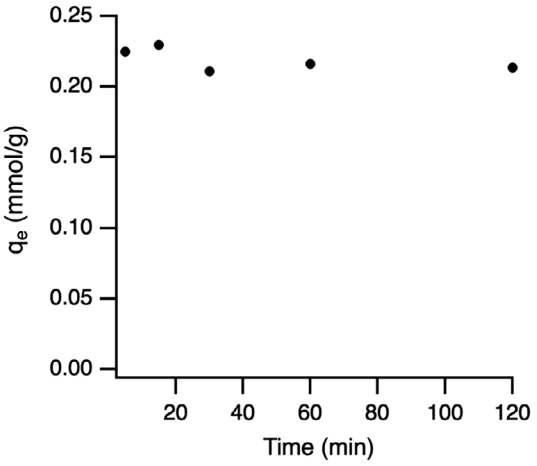

FIGURE 3 Acetic acid uptake as a function of time for 0.5 mmol/g primary amine-SBA-15

3.3 | Varying ligand loading

With the information above in hand subsequent work focused on the primary and quaternary functionalized materials as they showed the highest uptakes, likely for different physical reasons. Figure 4a shows the effect of ligand loading on uptake at a fixed acetic acid concentration of 0.087 M (0.5 vol%). In the case of the primary amine functionalized silicas, a simple linear increase in uptake was observed until 1 mmol/g, above which uptake plateaued. This corresponded to 18% of the amine sites binding acetic acid assuming a 1:1 complex, and acetic acid removal of 31%.

By contrast, it was difficult to make quaternary ammonium functionalized silicas with loadings above 1 mmol/g. We attributed this to the bulk of the quaternary ammonium group as well as the fact that this silane has a strong ionic character, which also inhibited high ligand densities on the surface. The quaternary ammonium samples were also less efficient; in the case of the highest loadings 11% of the sites bind acetic acid and there was a 7% removal of acetic acid.

It should also be noted that although values calculated from TGA results (weight loss curves shown in Figures S12 and S13) seen in Figure 4b showed a maximum loading at 1.5 mmol/g of amine

functional groups, it had been previously shown in literature that only ~30% of bound amines were accessible to probe molecules.[73] To confirm the loading of the primary amine grafted samples in this study, a ninhydrin assay for primary amines[72] was employed and showed (Figure S14) amine accessibility increasing from 30% at 0.1 mmol/g to a maximum of 50% at 0.5 mmol/g, consistent with previous studies.[49] The low accessibility was attributed to grafting preferentially at micropore openings, as SBA-15 is well known to have slight microporosity,[79] and polymeric layers forming at higher grafting densities that restrict access to the bulk solution.

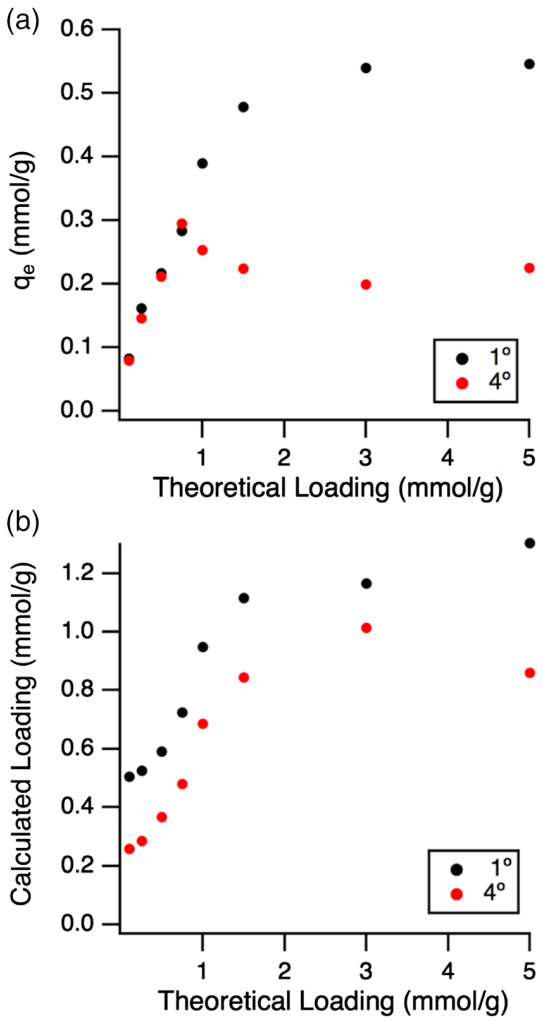

FIGURE 4 (a) Acetic acid uptake as a function of ligand loading during functionalization and (b) calculated ligand loading from TGA weight loss compared to theoretical aminosilane amount added during the functionalization step [Color figure can be viewed at wileyonlinelibrary.com]

3.4 | Pore size variation

The effect of mesopore size on uptake was determined by using MCM-41 as a support. The MCM-41 materials used had a nominal pore size of 3.7 nm, in contrast to the SBA-15 which had a pore size of 7.5 nm. Figure 5a shows the uptake comparison for the four types of aminosilicas grafted at 0.5 mmol/g on MCM-41. It can be observed in Figure 5b, that the MCM-41 functionalized materials had higher uptakes than the corresponding SBA-15 materials at 0.5 mmol/g ligand loading, with the exception of the primary amine. The modestly higher uptake observed for MCM-41 was attributed to confinement effects and increased surface area for loading of bulkier ligands (TGA comparison shown in Figure S15). Analysis of these samples via the Langmuir and Freundlich models is summarized in Table 2. Here the chi-squared values are similar for both models. It is interesting to note that the K_L values for the Langmuir model are higher as compared to the SBA-15 data in Table 1. One interpretation of this is that there is a stronger interaction in MCM-41 due to the smaller pore size as compared to SBA-15. The model fits to the experimental data can be seen in Figure S16.

3.5 | Recycle measurements

One issue that could complicate the results above is stability, specifically does the ligand become hydrolyzed from the surface due to the acetic acid? Figure 6 shows the uptake loss as the samples go through multiple cycles. The cycles were completed by washing the solid, obtained by centrifugation, from a standard uptake experiment six times with 20 ml of DI water and centrifuged after each washing. The resulting powder was dried under vacuum for 24 hr

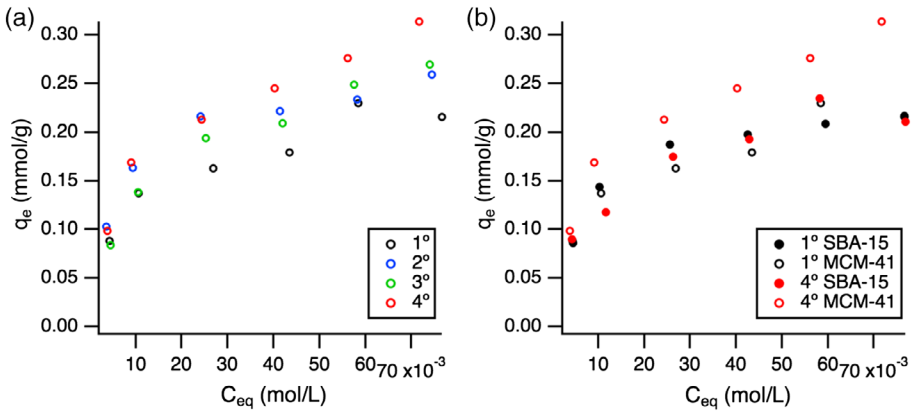

FIGURE 5 (a) Comparison of aminosilanes grafted to MCM-41for acetic acid uptake and (b) comparison of uptake on primary and quaternary amines for SBA-15 and MCM-41 [Color figure can be viewed at wileyonlinelibrary.com]

TABLE 2 Calculated fitting parameters for Langmuir and Freundlich fits of acetic acid uptake on amine-functionalized MCM-41 ($C_{eq} \leq 0.04$ M)

	Langmuir model			Freundlich model		
	K_L (L/Mol)	q_m (mmol/g)	χ^2	K_F	n	χ^2
1°	193.6 ± 9.1	0.199 ± 0.002	1.04×10^{-4}	0.428 ± 0.038	0.270 ± 0.023	8.0×10^{-4}
2°	191.7 ± 10.8	0.255 ± 0.004	2.54×10^{-4}	0.582 ± 0.067	0.286 ± 0.029	2.14×10^{-4}
3°	109.1 ± 4.5	0.259 ± 0.003	1.13×10^{-4}	0.810 ± 0.23	0.434 ± 0.073	4.91×10^{-4}
4°	150.9 ± 10.5	0.281 ± 0.006	4.51×10^{-4}	0.732 ± 0.074	0.334 ± 0.026	1.04×10^{-4}

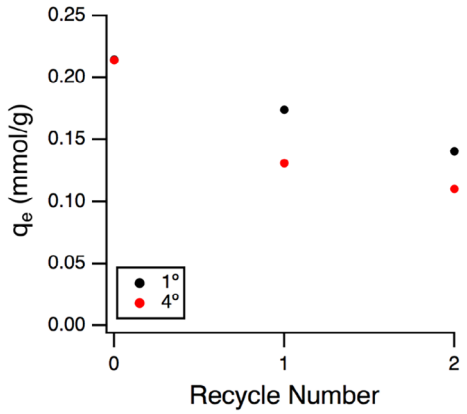

FIGURE 6 Equilibrium uptake of acetic acid for the primary and quaternary functionalized SBA-15 materials as a function of recycle [Color figure can be viewed at wileyonlinelibrary.com]

then a standard uptake measurement was completed. It should be noted there was always a slight mass loss during the washing steps. Interestingly, while there is clearly a modest loss of uptake capacity over multiple cycles, TGA results (Figure S17) show that there is negligible loss of ligand over multiple cycles. Thus, while there is clearly some loss of uptake capacity over the time scale of tens of hours, the differences in the samples observed in Figure 2 are not due to loss of ligand.

3.6 | Effects of solution conditions, other probe molecules

Multiple solution parameters were studied to determine the uptake mechanism. Figure 7a shows the effect of salt on acetic acid uptake. These experiments showed that the extraction mechanism was similar for both primary amine and quaternary ammonium grafted samples as the loss in uptake was similar. As the salt content increased acetic acid uptake decreased, consistent with electrostatic forces playing a role in uptake. By increasing the salt concentration, the effective length of the electrostatic force (Debye Length) was reduced resulting in a lower electrostatic potential farther away from the interface.

The effect of pH was also studied, the results of which are shown in Figure 7b. As one might expect the uptake decreased with increasing pH (adjusted with sodium acetate) and by the time a pH of seven was reached, the primary amine functionalized silica effectively did not take up acetic acid. This result showed that only the protonated acid was extracted for both samples and that no ion exchange for the quaternary amine salt occurred (the *pKa* of acetic acid is 4.75). This result combined with the salt and recycle experiments showed that the primary extraction mechanism was electrostatic due to the charge of the amine group and —OH group of the acetic acid.

3.7 | Competitive uptake

Experiments were performed to determine if the presence of competitor molecules perturbed acetic acid uptake. Figure 8a shows the uptake of acetic acid over the various aminosilicas in the presence of dextrose. Interestingly a modest enhancement of acetic acid uptake was observed for all samples. Figure 8b then shows how the acetic acid uptake varied for the primary and quaternary samples as the dextrose concentration was varied. A modest increase in acetic acid uptake was observed as the dextrose concentration was increased. The reason for this was likely a formation of a complex between acetic acid and dextrose due to the hydroxyl groups of the dextrose and the protonated acid group of the acetic acid. This resulted in a more electrophilic molecule causing a stronger interaction with the basic amine groups. A similar phenomenon had been described previously with boronic acid and diol containing molecules.[80]

Figure 9a shows the uptake of three different acids: acetic, butyric, and hexanoic, from solution as a function of individual acid concentration. The acid molar ratios were 1:1:1 in the initial solution. For comparison purposes, uptake of each pure acid at 0.05 M is shown in Figure 9b. The simple conclusion from these figures is that the more hydrophobic the acid, the more efficiently it is captured from solution. Acetic acid and butyric acid uptake were lower in the mixtures as compared to uptake from solutions of a single acid. When comparing how much acid was removed from the mixed solution at 0.05 M each, 10% acetic, 14% butyric, and 46% hexanoic acid were removed which represents 23% of the total acid in solution removed. Finally, it should be pointed out that one reason for the low total concentrations of acid used here is that the hexanoic acid has a low solubility in water, 0.968 g/100 ml.[81]

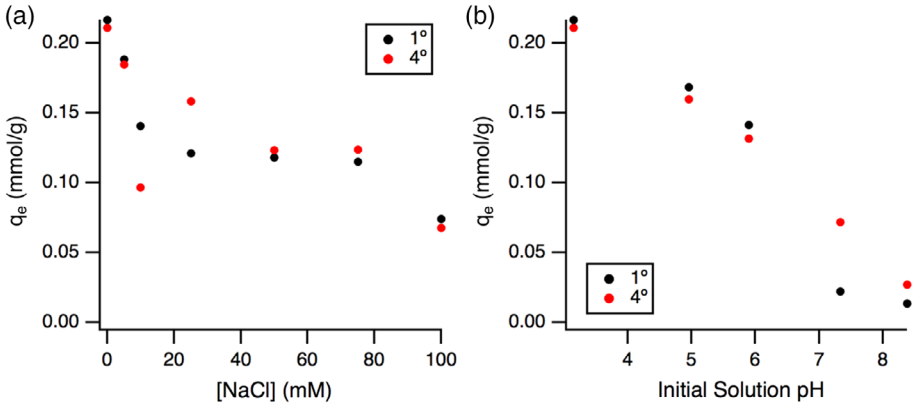

FIGURE 7 (a) The effect of salt on acetic acid uptake for the primary and quaternary samples and (b) acetic acid uptake for the quaternary and primary samples as a function of solution pH [Color figure can be viewed at wileyonlinelibrary.com]

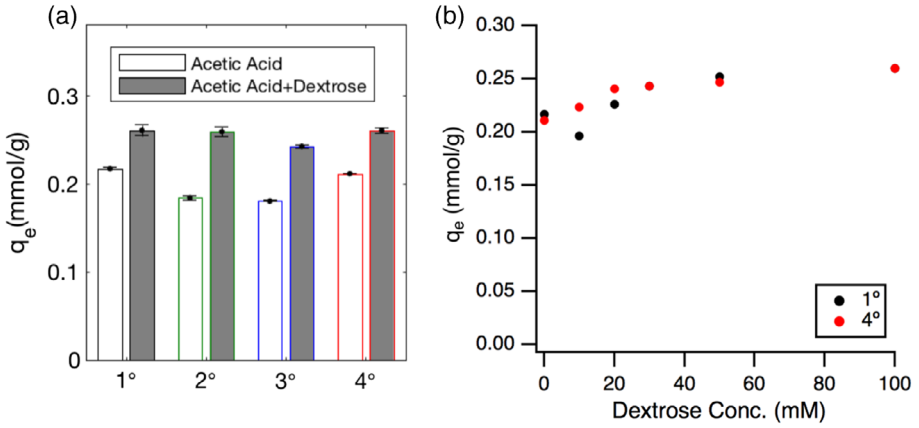

FIGURE 8 (a) The effect of dextrose on the uptake of acetic acid from 0.5 vol% solutions and (b) variation of acetic acid uptake as a function of dextrose concentration [Color figure can be viewed at wileyonlinelibrary.com]

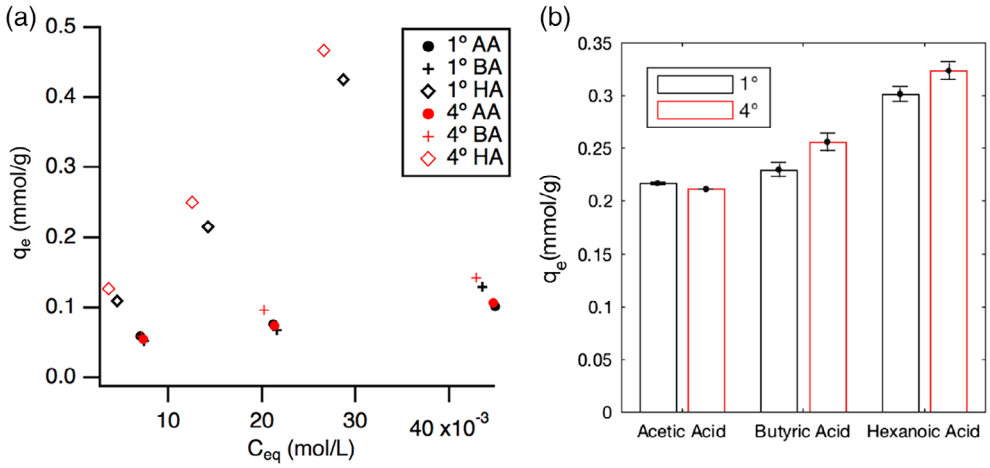

FIGURE 9 (a) Uptake results for acetic, butyric, and hexanoic acid as a function of individual acid concentration. For a given uptake experiment all three acids are present in a 1:1:1 M ratio and (b) uptake of each pure carboxylic acid at a concentration of 0.05 M. The ligand loading was held constant at 0.5 mmol/g on SBA-15 [Color figure can be viewed at wileyonlinelibrary.com]

4 | CONCLUSIONS

The current work provides a full picture of the macroscopic uptake properties of acetic acid, an undesirable byproduct of biomass depolymerization. Clear trends emerge as to how the degree of methylation influences acetic acid uptake. The effects of solution conditions are also reported, as well as how the presence of competitor molecules influences uptake properties. From these results it is clear that uptake depends on the electrostatic charge on the amine, polarity of the amine and acid, and the dissociation constant of the amine and acid. The inorganic support also plays a crucial role in that ligand loading can differ based on the support's pore size and volume, which can increase or decrease the loading based on the ligand's steric bulk and charge. This work provides a foundational basis for developing deeper insights into how model adsorbent materials can be used to remove dilute species from aqueous media. Ongoing work is probing the

binding dynamics of acetic acid at the molecular level and will be reported elsewhere.

ACKNOWLEDGMENTS

The authors gratefully acknowledge support from NSF award 1703251.

ORCID

Daniel F. Shantz https://orcid.org/0000-0002-3237-6120

REFERENCES

1. Hoffmann F, Cornelius M, Morell J, Fröba M. Silica-based mesoporous organic–inorganic hybrid materials. *Angew Chem Int Ed*. 2006;45(20):3216-3251.
2. Sanchez C, Julián B, Belleville P, Popall M. Applications of hybrid organic–inorganic nanocomposites. *J Mater Chem*. 2005;15(35–36):3559-3592.
3. Stein A, Melde BJ, Schroden RC. Hybrid inorganic–organic mesoporous silicates—nanoscopic reactors coming of age. *Adv Mater*. 2000;12(19):1403-1419.
4. Judeinstein P, Sanchez C. Hybrid organic–inorganic materials: a land of multidisciplinarity. *J Mater Chem*. 1996;6(4):511-525.
5. Cheetham AK, Rao C, Feller RK. Structural diversity and chemical trends in hybrid inorganic–organic framework materials. *Chem Commun*. 2006;46:4780-4795.
6. Sayari A, Hamoudi S. Periodic mesoporous silica-based organic– inorganic nanocomposite materials. *Chem Mater*. 2001;13(10):3151-3168.
7. Sanchez C, Lebeau B, Chaput F, Boilot JP. Optical properties of functional hybrid organic–inorganic nanocomposites. *Adv Mater*. 2003;15(23):1969-1994.
8. Feng X, Fryxell G, Wang L-Q, Kim AY, Liu J, Kemner K. Functionalized monolayers on ordered mesoporous supports. *Science*. 1997;276(5314):923-926.
9. Moller K, Bein T. Inclusion chemistry in periodic mesoporous hosts. *Chem Mater*. 1998;10(10):2950-2963.
10. Ford DM, Simanek EE, Shantz DF. Engineering nanospaces: ordered mesoporous silicas as model substrates for building complex hybrid materials. *Nanotechnology*. 2005;16(7):S458.
11. Anwander R, Nagl I, Widenmeyer M, et al. Surface characterization and functionalization of MCM-41 silicas via silazane silylation. *J Phys Chem B*. 2000;104(15):3532-3544.
12. Hiyoshi N, Yogo K, Yashima T. Adsorption characteristics of carbon dioxide on organically functionalized SBA-15. *Micropor Mesopor Mat*. 2005;84(1–3):357-365.
13. Wang J, Huang L, Yang R, et al. Recent advances in solid sorbents for CO 2 capture and new development trends. *Energ Environ Sci*. 2014;7(11):3478-3518.
14. Zelenak V, Halamova D, Gaberova L, Bloch E, Llewellyn P. Amine-modified SBA-12 mesoporous silica for carbon dioxide capture: effect of amine basicity on sorption properties. *Micropor Mesopor Mat*. 2008;116(1–3):358-364.
15. Samanta A, Zhao A, Shimizu GK, Sarkar P, Gupta R. Post-combustion CO_2 capture using solid sorbents: a review. *Ind Eng Chem Res*. 2011;51(4):1438-1463.
16. Choi S, Gray ML, Jones CW. Amine-tethered solid adsorbents coupling high adsorption capacity and regenerability for CO_2 capture from ambient air. *ChemSusChem*. 2011;4(5):628-635.
17. Ko YG, Shin SS, Choi US. Primary, secondary, and tertiary amines for CO_2 capture: designing for mesoporous CO_2 adsorbents. *J Colloid Interface Sci*. 2011;361(2):594-602.
18. Lee JJ, Chen C-H, Shimon D, Hayes SE, Sievers C, Jones CW. Effect of humidity on the CO_2 adsorption of tertiary amine grafted SBA-15. *J Phys Chem C*. 2017;121(42):23480-23487.
19. Didas SA, Kulkarni AR, Sholl DS, Jones CW. Role of amine structure on carbon dioxide adsorption from ultradilute gas streams such as ambient air. *ChemSusChem*. 2012;5(10):2058-2064.
20. Sayari A, Belmabkhout Y, Da'na E. CO_2 deactivation of supported amines: does the nature of amine matter? *Langmuir*. 2012;28(9):4241-4247.
21. Okonkwo CN, Okolie C, Sujan A, Zhu G, Jones CW. Role of amine structure on hydrogen sulfide capture from dilute gas streams using solid adsorbents. *Energy & Fuels*. 2018;32:6926-6933
22. Fan Y, Rezaei F, Labreche Y, Lively RP, Koros WJ, Jones CW. Stability of amine-based hollow fiber CO_2 adsorbents in the presence of NO and SO_2. *Fuel*. 2015;160:153-164.
23. Nomura A, Jones CW. Amine-functionalized porous silicas as adsorbents for aldehyde abatement. *ACS Appl Mater Interfaces*. 2013;5(12):5569-5577.
24. Shylesh S, Hanna D, Gomes J, et al. Tailoring the cooperative acid–base effects in silica-supported amine catalysts: applications in the continuous gas-phase self-condensation of n-butanal. *ChemCatChem*. 2014;6(5):1283-1290.
25. Aguado J, Arsuaga JM, Arencibia A, Lindo M, Gascón V. Aqueous heavy metals removal by adsorption on amine-functionalized mesoporous silica. *J Hazard Mater*. 2009;163(1):213-221.
26. Hernández-Morales V, Nava R, Acosta-Silva Y, Macías-Sánchez S, Pérez-Bueno J, Pawelec B. Adsorption of lead (II) on SBA-15 mesoporous molecular sieve functionalized with–NH_2 groups. *Micropor Mesopor Mat*. 2012;160:133-142.
27. Jrm H, Palacio R, Safizadeh F, et al. Adsorption of uranium over NH2-functionalized ordered silica in aqueous solutions. *ACS Appl Mater Interfaces*. 2017;9(18):15672-15684.
28. Ho KY, McKay G, Yeung KL. Selective adsorbents from ordered mesoporous silica. *Langmuir*. 2003;19(7):3019-3024.
29. Choi J-W, Lee S-Y, Chung S-G, Hong S-W, Kim D-J, Lee S-H. Removal of phosphate from aqueous solution by functionalized mesoporous materials. *Water, Air, & Soil Pollut*. 2011;222(1–4):243-254.
30. Hamoudi S, El-Nemr A, Belkacemi K. Adsorptive removal of dihydrogenphosphate ion from aqueous solutions using mono, di-and tri-ammonium-functionalized SBA-15. *J Colloid Interface Sci*. 2010;343(2):615-621.
31. Yoshitake H. Design of functionalization and structural analysis of organically-modified siliceous oxides with periodic structures for the development of sorbents for hazardous substances. *J Mater Chem*. 2010;20(22):4537-4550.
32. Walcarius A, Mercier L. Mesoporous organosilica adsorbents: nanoengineered materials for removal of organic and inorganic pollutants. *J Mater Chem*. 2010;20(22):4478-4511.
33. Jun Y-S, Huh YS, Park HS, et al. Adsorption of pyruvic and succinic acid by amine-functionalized SBA-15 for the purification of succinic acid from fermentation broth. *J Phys Chem C*. 2007;111(35):13076-13086.
34. Sedai B, Zhou JL, Fakhri N, Sayari A, Baker RT. Solid phase extraction of bio-oil model compounds and lignin-derived bio-oil using amine-functionalized mesoporous silicas. *ACS Sustain Chem Eng*. 2018;6:9716-9724
35. Bozell JJ. Connecting biomass and petroleum processing with a chemical bridge. *Science*. 2010;329(5991):522-523.
36. Corma A, Iborra S, Velty A. Chemical routes for the transformation of biomass into chemicals. *Chem Rev*. 2007;107(6):2411-2502.
37. Huber GW, Iborra S, Corma A. Synthesis of transportation fuels from biomass: chemistry, catalysts, and engineering. *Chem Rev*. 2006;106(9):4044-4098.
38. Regalbuto JR. Cellulosice biofuels-got gasoline? *Science*. 2009;325:822-824.
39. Richard TL. Challenges in scaling up biofuels infrastructure. *Science*. 2010;329:793-796.
40. Willems PA. The biofuels landscape through the lens of industrial chemistry. *Science*. 2009;325:707-708.
41. Antal MJ, Varhegyi G. Cellulose pyrolysis kinetics—The current state of knowledge. *Ind Eng Chem Res*. 1995;34(3):703-717.

42. Branca C, Giudicianni P, Di Blasi C. GC/MS characterization of liquids generated from low-temperature pyrolysis of wood. *Ind Eng Chem Res*. 2003;42(14):3190-3202.
43. Graham RG, Bergougnou MA, Overend RP. Fast pyrolysis of biomass. *J Anal Appl Pyrol*. 1984;6(2):95-135.
44. Lin YC, Huber GW. The critical role of heterogeneous catalysis in lignocellulosic biomass conversion. *Energ Environ Sci*. 2009;2(1):68-80.
45. Mohan D, Pittman CU, Steele PH. Pyrolysis of wood/biomass for bio-oil: a critical review. *Energy Fuel*. 2006;20(3):848-889.
46. Sun Y, Cheng J. Hydrolysis of lignocellulosic materials for ethanol production: a review. *Bioresour Technol*. 2002;83(1):1-11.
47. Yung MM, Jablonski WS, Magrini-Bair KA. Review of catalytic conditioning of biomass-derived syngas. *Energy Fuel*. 2009;23:1874-1887.
48. Tung LA, King CJ. Sorption and extraction of lactic and succinic acids at pH> pKa1. I. Factors governing equilibria. *Ind Eng Chem Res*. 1994;33(12):3217-3223.
49. Eyal AM, Canari R. pH dependence of carboxylic and mineral acid extraction by amine-based extractants: effects of pKa, amine basicity, and diluent properties. *Ind Eng Chem Res*. 1995;34(5):1789-1798.
50. Canari R, Eyal AM. Extraction of carboxylic acids by amine-based extractants: apparent extractant basicity according to the pH of half-neutralization. *Ind Eng Chem Res*. 2003;42(7):1285-1292.
51. Canari R, Eyal AM. Selectivity in monocarboxylic acids extraction from their mixture solutions using an amine-based extractant: effect of pH. *Ind Eng Chem Res*. 2003;42(7):1301-1307.
52. Tamada JA, Kertes AS, King CJ. Extraction of carboxylic acids with amine extractants. 1. Equilibria and law of mass action modeling. *Ind Eng Chem Res*. 1990;29(7):1319-1326.
53. Tamada JA, King CJ. Extraction of carboxylic acids with amine extractants. 2. Chemical interactions and interpretation of data. *Ind Eng Chem Res*. 1990;29(7):1327-1333.
54. Tamada JA, King CJ. Extraction of carboxylic acids with amine extractants. 3. Effect of temperature, water coextraction, and process considerations. *Ind Eng Chem Res*. 1990;29(7):1333-1338.
55. Canari R, Eyal AM. Temperature effect on the extraction of carboxylic acids by amine-based extractants. *Ind Eng Chem Res*. 2004;43(23):7608-7617.
56. Kertes A, King CJ. Extraction chemistry of fermentation product carboxylic acids. *Biotechnol Bioeng*. 1986;28(2):269-282.
57. Kirsch T, Maurer G. Distribution of binary mixtures of citric, acetic and oxalic acid between water and organic solutions of tri-n-octylamine: part II. Organic solvent methylisobutylketone. *Fluid Phase Equil*. 1998;142(1–2):215-230.
58. Kirsch T, Maurer G. Distribution of binary mixtures of citric, acetic and oxalic acid between water and organic solutions of tri-n-octylamine part I. Organic solvent toluene. *Fluid Phase Equil*. 1997;131(1–2):213-231.
59. Kirsch T, Maurer G. Distribution of binary mixtures of citric, acetic and oxalic acid between water and organic solutions of tri-n-octylamine: part III. Organic solvent chloroform. *Fluid Phase Equil*. 1998;146(1–2):297-313.
60. Shan X, Qin W, Dai Y. Dependence of extraction equilibrium of monocarboxylic acid from aqueous solutions on the relative basicity of extractant. *Chem Eng Sci*. 2006;61(8):2574-2581.
61. Grzenia DL, Schell DJ, Wickramasinghe SR. Membrane extraction for removal of acetic acid from biomass hydrolysates. *J Membr Sci*. 2008;322(1):189-195.
62. Kyuchoukov G, Yankov D, Albet J, Molinier J. Mechanism of lactic acid extraction with quaternary ammonium chloride (Aliquat 336). *Ind Eng Chem Res*. 2005;44(15):5733-5739.
63. Mandal B, Bandyopadhyay S. Absorption of carbon dioxide into aqueous blends of 2-amino-2-methyl-1-propanol and monoethanolamine. *Chem Eng Sci*. 2006;61(16):5440-5447.
64. Torget R, Walter P, Himmel M, Grohmann K. Dilute-acid pretreatment of corn residues and short-rotation woody crops. *Appl Biochem Biotechnol*. 1991;28(1):75.
65. Mullen CA, Boateng AA. Chemical composition of bio-oils produced by fast pyrolysis of two energy crops. *Energy Fuel*. 2008;22(3):2104-2109.
66. Zhao D, Huo Q, Feng J, Chmelka BF, Stucky GD. Nonionic triblock and star diblock copolymer and oligomeric surfactant syntheses of highly ordered, hydrothermally stable, mesoporous silica structures. *J Am Chem Soc*. 1998;120(24):6024-6036.
67. Edler K, White J. Further improvements in the long-range order of MCM-41 materials. *Chem Mater*. 1997;9(5):1226-1233.
68. Zhao D, Feng J, Huo Q, et al. Triblock copolymer syntheses of mesoporous silica with periodic 50 to 300 angstrom pores. *Science*. 1998;279(5350):548-552.
69. Beck JS, Vartuli J, Roth WJ, et al. A new family of mesoporous molecular sieves prepared with liquid crystal templates. *J Am Chem Soc*. 1992;114(27):10834-10843.
70. Evans J, Zaki A, El-Sheikh M, El-Safty S. Incorporation of transition-metal complexes in functionalized mesoporous silica and their activity toward the oxidation of aromatic amines. *J Phys Chem B*. 2000;104(44):10271-10281.
71. Fadeev AY, McCarthy TJ. Trialkylsilane monolayers covalently attached to silicon surfaces: wettability studies indicating that molecular topography contributes to contact angle hysteresis. *Langmuir*. 1999;15(11):3759-3766.
72. Soto-Cantu E, Cueto R, Koch J, Russo PS. Synthesis and rapid characterization of amine-functionalized silica. *Langmuir*. 2012;28(13):5562-5569.
73. Ritter H, Brühwiler D. Accessibility of amino groups in post-synthetically modified mesoporous silica. *J Phys Chem C*. 2009;113(24):10667-10674.
74. Mizukami M, Nakagawa Y, Kurihara K. Surface induced hydrogen-bonded macrocluster formation of methanol on silica surfaces. *Langmuir*. 2005;21(21):9402-9405.
75. Parida SK, Dash S, Patel S, Mishra B. Adsorption of organic molecules on silica surface. *Adv Colloid Interface Sci*. 2006;121(1–3):77-110.
76. DeJaco RF, de Mello MD, Nguyen HGT, et al. Vapor and liquid phase adsorption of alcohol and water in Silicalite-1 synthesized in fluoride media. *AIChE J*. 2019 e16868. https://doi.org/10.1002/aic.16868.
77. Langmuir I. The adsorption of gases on plane surfaces of glass, mica and platinum. *J Am Chem Soc*. 1918;40(9):1361-1403.
78. Freundlich H. *Colloid & Capillary Chemistry*. London, Methuen & Co. Ltd; 1926.
79. Ravikovitch PI, Neimark AV. Characterization of micro-and mesoporosity in SBA-15 materials from adsorption data by the NLDFT method. *J Phys Chem B*. 2001;105(29):6817-6823.
80. Springsteen G, Wang B. A detailed examination of boronic acid–diol complexation. *Tetrahedron*. 2002;58(26):5291-5300.
81. Ralston A, Hoerr C. The solubilities of the normal saturated fatty acids. *J Org Chem*. 1942;7(6):546-555.

SUPPORTING INFORMATION

Additional supporting information may be found online in the Supporting Information section at the end of this article.

How to cite this article: Miller PJ, Shantz DF. Amine-functionalized ordered mesoporous silicas as model materials for liquid phase acid capture. *AIChE J*. 2020;66:e16918. https://doi.org/10.1002/aic.16918